This is the accepted manuscript made available via CHORUS. The article has been published as:

# Universality Class of Nanocrystal Plasticity: Localization and Self-Organization in Discrete Dislocation Dynamics

Hengxu Song, Dennis Dimiduk, and Stefanos Papanikolaou

Phys. Rev. Lett. **122**, 178001 — Published 3 May 2019

DOI: 10.1103/PhysRevLett.122.178001

# The Universality Class of Nano-Crystal Plasticity: Localization and Self-Organization in Discrete Dislocation Dynamics

Hengxu Song,[1] Dennis Dimiduk,[2] and Stefanos Papanikolaou*[1,3]

[1]*Department of Mechanical and Aerospace Engineering, West Virginia University, Morgantown, WV26506, United States.*
[2]*Department of Materials Science Engineering, Ohio State University, Columbus, OH43210, United States.*
[3]*Department of Physics, West Virginia University, Morgantown, WV26506, United States.*

(Dated: March 26, 2019)

The universality class of the avalanche behavior in plastically deforming crystalline and amorphous systems has been commonly discussed, despite the fact that the microscopic defect character in each of these systems is different. In contrast to amorphous systems, crystalline flow stress increases dramatically at high strains and/or loading rates. We perform simulations of a two-dimensional discrete dislocation dynamics model that minimally captures the phenomenology of nano-crystalline deformation. In the context of this model, we demonstrate that a classic rate-dependence of dislocation plasticity at large rates ($> 10^3/s$), fundamentally controls the system's statistical character as it competes with dislocation nucleation: At large rates, the behavior is statistically dominated by long-range correlations of "dragged" mobile dislocations. At small rates, plasticity localization dominates in small volumes and a spatial integration of avalanche behaviors takes place.

Crystal plasticity in small volumes has been investigated in the last two decades through the compression of micro and nano-pillars [1–6]. In these small volumes, the material strength is size-dependent due to strain gradients[7–17] generated by unconventional dislocation generation and motion mechanisms. Furthermore, macroscopic work hardening [18, 19] is replaced by a wealth of abrupt plastic events [20–24] that originate in both the presence of dislocation correlations, as well as the dramatic small volume effect of mobile dislocations forming geometric steps on free pillar surfaces [21, 22, 25–27]. Abrupt plastic events are common in avalanche phenomena of various disordered non-equilibrium systems across length scales [28–32], especially elastic interface depinning phenomena, with which crystals share similar, but not identical, avalanche statistics [33]. However, in common crystal "depinning" modeling attempts [34–38], avalanches are caused by a direct competition of elastic loading and long-range elastic interactions with quenched disorder, without temporal bursts in the number of elastic degrees of freedom. In contrast, dislocations in nanocrystals can also nucleate, multiply and deposit on free boundaries [5, 39, 40], naturally causing additional frustration that may influence the statistical avalanche behavior [37, 41–43]. Here, in the context of an explicit dislocation dynamics model, we show that the competition between two different ways to mediate plastic slip – dislocation nucleation and over-damped dislocation mobility (*ie.* dislocation drag) – leads to a distinct rate effect on the avalanche statistics that becomes more pronounced for stress-controlled loading conditions. We interpret the phenomenon in terms of a spatial integration of avalanche behaviors across slip planes [41]. This is a generic mechanism in bifurcation processes such as the Frank-Read nucleation of a single dislocation, and thus we argue that the proposed effect should extend to 3D-DDD models [32, 44].

Dislocation avalanches [45] have been observed experimentally in diameter-$D$ micro and nano pillar compression studies [21, 46, 47] where power law statistics for the sizes $S$ of the form $P(S) = S^{-\tau}\mathcal{P}(S/S_0)$ has been established, where $\tau \in (1.2, 1.8)$, $S_0 \sim D$ and $\mathcal{P}$ resembles an exponential cutoff function [48]. Two [33, 49–61] and three [6, 27, 49, 62–65] dimensional models of atomic displacements or/and discrete dislocations simulations[33, 49, 51, 66, 67] have established that $\tau \sim 1.5$ [68] or lower [56], regardless of loading protocols [20, 28], even if there are still various issues on how the statistics is estimated [32, 33, 58]. However, recent 3D Discrete Dislocation Dynamics (3D-DDD) studies [44] showed that avalanche statistics strongly depend on the loading protocol, where power law statistics with $\tau \sim 1.5$ only exhibited in stress-controlled (SC) loading. In addition, recent experiments and continuum modeling [41, 69, 70] suggest that $\tau$ may take much larger values, originating in internal disorder or/and thermal relaxation mechanisms such as cross-slip.

The effect of loading protocols on the statistical behavior of nano-pillar compression has been studied recently [71, 72], even though the connection between stress rate $\dot{\sigma}$ (in SC) and strain rate $\dot{\epsilon}$ (in displacement-controlled loading (DC)) has been lacking at small rates. In contrast, at large loading rates ($> 10^3/s$) and in the macro-scale, crystals exhibit a sharp increase of the flow stress due to viscoplastic *dislocation drag effects* when strain rate surpasses $\sim 5000/s$ [73–76]. This fact is verified in DDD simulations [77, 78] and originates in the natural competition between the timescale for a dislocation to move a minimal distance at terminal speed and the timescale for dislocation "nucleation" (*eg.* at a Frank-Read source) [79]. How does this competition translate to the statistical behavior of plasticity avalanches in small volumes at rates smaller than $10^3$/s?

In this paper, we consider a *minimal* model of crystal plasticity for uniaxial compression in small volumes. By "minimal", we imply a model that respects: i) the energetics of room temperature crystal deformation being mediated by dislocations gliding along slip planes of at least one slip system ii) the fact that small-volume crystalline plastic deformation originates in nucleation, iii) open boundaries absorb dislocations , iv) competing dislocation kinetics mechanisms. In order to maximize statistical sampling and computational efficiency, we perform simulations of 2D samples using a benchmarked dislocation dynamics model [80, 81] that displays the basic phenomenology of nano-crystalline compression: Size effects in the material yield strength and emergent crackling noise. For pure elasticity, SC and DC loading modes can be compared by using $\dot{\sigma} = E^*\dot{\epsilon}$, where $E^* = \frac{E}{1-\nu^2}$ is the equivalent modulus for plane strain applications and $\nu$ is the Poisson's ratio. The loading strain-rate $\dot{\epsilon}$ is varied from 10/s to $10^5$/s. The model crystal is initially stress and mobile-dislocation free. This is analogous to a well-annealed sample, yet with pinned dislocation segments that can act either as dislocation sources (*eg.* Frank Read sources) or as obstacles. Dislocations are generated from randomly distributed point sources when the resolved shear stress crosses a random threshold $\tau_{\rm nuc}$ for a finite time $\delta t_{\rm nuc} = 10ns$ [95]. The nucleated dislocation pair is placed at a distance $L_{\rm nuc} = E/(4\pi(1-\nu^2))b/\tau_{\rm nuc}$ and for our system parameters, it is $35nm$ on average [96]. Randomly distributed point obstacles account for precipitates and forest dislocations on out-of-plane slip systems. These obstacles are minimal with only athermal pinning criteria to avoid the interplay with additional timescales. Microstructural parameters are chosen based on a previous study [80] that matches various experimental facts. All simulation parameters are listed in Table I.

TABLE I: **Model Parameters**: The model is designed to reasonably display the phenomenology of uniaxial nanopillar compression experiments [80], with parameters for the slip plane spacing $d$, slip plane orientation $\theta$ respective to the loading direction, source density $\rho_{\rm nuc}$, average source strength $\bar{\tau}_{\rm nuc}$ and its standard deviation (SDV), nucleation time $t_{\rm nuc}$, obstacle density $\rho_{\rm obs}$, average obstacle strength $\bar{\tau}_{\rm obs}$ and its SDV.

| slip planes | sources | obstacles |
|---|---|---|
| $d$=10$b$ | $\rho_{\rm nuc}$=60$\mu m^{-2}$ | $\rho_{\rm obs}$=480MPa |
| $\theta = 30°$ | $\bar{\tau}_{\rm nuc}$ =50MPa | $\bar{\tau}_{\rm obs}$ =150MPa |
| | $\delta\tau_{\rm nuc}$ =5MPa | $\delta\tau_{obs}$ =20MPa |

The timescale competition in this model is generic and present not only in all dislocation dynamics models, but also in generic non-equilibrium processes [82]. Its basic origin can be distilled by considering an imperfect pitchfork bifurcation: $d\epsilon/dt = \sigma + \mu\epsilon - \epsilon^3$, where $\epsilon, \sigma$ are scalars resembling strain and stress variables, and $\mu$ is a mobility parameter. Neglecting dislocation interactions, on a slip plane without sources but a mobile dislocation, $\mu = \mu_{\rm drift}$ is negative and the relaxation timescale for *every* incremental step of $\sigma$ is $\delta t_{\rm drift} = |\mu_{\rm drift}|^{-1}$. However, if a dislocation source is present without any mobile dislocations, then $\mu = \mu_{\rm nuc} > 0$ due to the existence of the two states with and without a dislocation pair, and the relaxation timescale during dislocation increments is $\delta t_{\rm nuc} = \mu_{\rm nuc}^{-1}$. Typically, $\delta t_{\rm nuc} \gg \delta t_{\rm drift}$, so increments of $\sigma$ will be accommodated by nucleation events. However, if a system of such possible bifurcations interact (if multiple dislocation sources are present), then mutual dislocation interactions may cause a frustrating situation where the disparity of relaxation times may cause a complexity in the evolution dynamics. In our DDD model, the two timescales are concerned with the nucleation and propagation of single dislocations.

Driven by local stress-induced forces [79], dislocations follow athermal dynamics with mobility $\mu_d$. Sample lateral surfaces are free for dislocations to escape from the surfaces. Samples (aspect ratio $h/w = 4$) are assumed to carry single slip plasticity oriented at 30° (*cf.* Fig. 1(a)). Dislocation sources (red dots) and obstacles (blue dots) are located on slip planes, spaced 10$b$ apart, with $b$ = 0.25nm the Burgers vector's length. The Young's modulus is assumed $E$ = 70 GPa and $\nu$ = 0.33. As it may be seen in Fig. 1(b), a significant difference between two loading rates (SC) can be seen through strain patterning at the same final strain (5%): plasticity is localized (Fig. 1(c)) for small loading rates while it is relatively uniform for a high loading rate (Fig. 1(d)).

As expected and shown in Fig. 2 (a), SC leads to hardening while DC to softening, with the discrepancy becoming dramatic as system size decreases to sub-micron dimensions. Typical size effects ($\sigma_Y \sim w^{-0.4-0.6}$) are seen for both loading protocols (*cf.* Fig. 2(b)), despite the fact that dislocation density at 2% strain, shown in the inset, increases with increasing $w$ in different ways depending on the loading conditions. In addition, the flow stress shows a rate dependence for both loading conditions (see Fig. 2(c)), even though DC shows weaker dependence. The origin of the discrepancy at small rates is that plasticity will be dominated by the weakest dislocation source in DC while in SC, stress increases consistently and monotonously, eventually triggering more dislocation sources, towards a collective dislocation response (see also Supplementary Information (SI)).

The dislocation density and flow stress dependences on the rate suggest that SC rates *statistically resemble* larger DC rates. This conclusion is also supplemented by avalanche statistics (*cf.* Fig. 2(d)): In SC, event size is defined as $S = \sum_{i \,\in\, \{\delta\epsilon^i > \epsilon_{\rm threshold}\}} \delta\epsilon^i$; in DC, an event is characterized by stress drops $\delta\sigma$ which lead to temporary displacement overshoots – thus, in order to compare the two loading conditions, a DC strain burst event size is defined as $S = \sum_{i \,\in\, \{-\delta\sigma^i > \sigma_{\rm threshold}\}} \delta\epsilon^i$ [44].

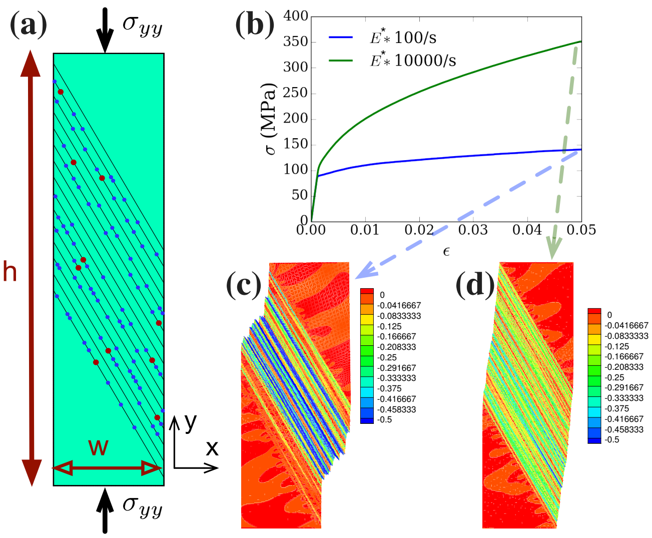


FIG. 1: **The model.** **(a)** The pillar has width $w$ and aspect ratio $h/w$=4. Single slip system which oriented at 30° relative to y axis is used. Distance between planes is $10b$ where $b$ = 0.25nm is the magnitude of the Burgers vector. Red dots stand for dislocation sources while blue dots represent dislocation obstacles. **(b)** Sample stress strain curves of compression at high ($10^5$/s) and low ($10^2$/s) stress rates $\dot{\sigma}$. **(c)** strain pattern after deformation at low $\dot{\sigma}$, **(d)** strain pattern after deformation at high $\dot{\sigma}$.

In this model, dislocation plasticity is loading rate dependent as there are two intrinsic time scales [77]: First, the dislocation nucleation time $\delta t_{\rm nuc}$, which is chosen as 10 $ns$ and can be associated to the dislocation multiplication timescale in other models. Second, the ratio between dislocation mobility and material Young's modulus $B/E$ which is chosen as $10^{-6}$ ns ($B = 10^{-4} Pa \cdot s$). These parameters are consistent with recent single-crystal thin film experiments [83, 84]. Phenomenology in metallurgy [75, 85, 86], suggests that at low rates the flow stress is controlled by dislocation nucleation while above a certain strain rate ($\sim 1000-5000$/s), it is mainly controlled by dislocation drag. Fig. 2(c) shows the rate effect under SC and DC conditions. For DC and at strain rates higher than 5000/s, there is a strong flow stress rate dependence. In SC, the drag regime starts when stress rate is $E^* * 10^2$/s. The origin of this strain-rate crossover is hidden in the amount of the strain that nucleation events can acommodate, with $\dot{\epsilon} > 10^3/s$ forcing dislocation drag to take over the dynamics of dislocations (see SI).

While both DC and SC display a flow stress rate effect, their statistical noise behavior is very different: As shown in Fig. 2(d), the plastic events statistics based on stress strain curves shown in Fig. 2(a), have different $\tau$ exponents: While plastic events show power law behavior, $\tau$ is close to 3.5 for DC and 1.5 for SC.

The avalanche size distribution exponent discrepancy between SC and DC disappears at high stress load-

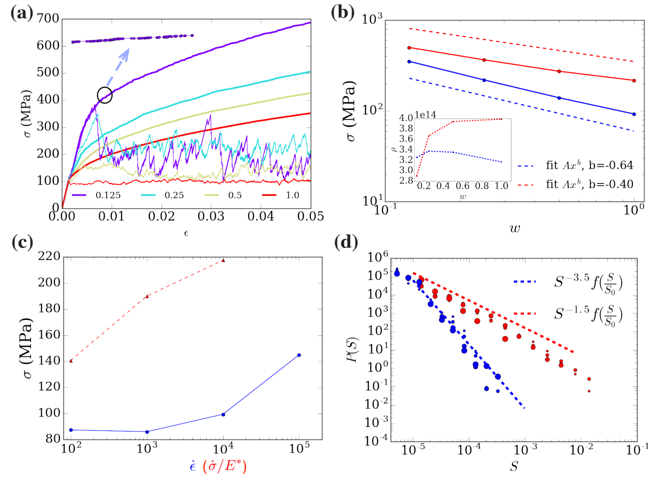


FIG. 2: **Effect of loading protocol: Stress-Controlled (SC) vs. Displacement-Controlled (DC).** **(a)** Stress-strain curves of different $w$ using two different loading protocols. The strain rate $\dot{\epsilon}$ is $10^4$/s in DC and stress rate $\dot{\sigma}$ is $E^* * 10^4$/s. A particular strain burst is shown; **(b)** Size effect of flow stress at 2% strain (blue stands for DC and red stand for SC, results are based on 50 realizations). The inset shows the dependence of dislocation density on $w$ at 2% strain for different loading protocols. **(c)** Dependence of flow stress (for $w = 1\mu$m) on rate. Strain rate $\dot{\epsilon}$ is used in DC (blue curve) while the elastic corresponding stress rate $\dot{\sigma} = E^*\dot{\epsilon}$ is used in SC (red curve). **(d)**: Events (strain jumps) statistics for different loading protocols, different point size represents different $w$. blue: DC, red: SC. Strain jump in DC mode is calculated according to the method in [44].

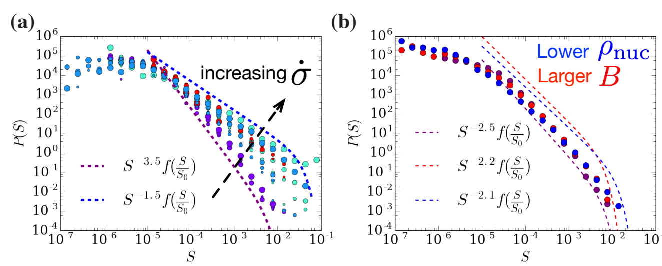


FIG. 3: **SC Rate Effect Crossover.** **(a):** Event statistics for different $\dot{\sigma}$ using SC. The effective $\tau$ changes from $\sim 3.5$ for $\dot{\sigma} = E^* * 10$/s to $\sim -1.5$ for $\dot{\sigma} = E^* * 10^4$/s. **(b):** Effect of dislocation source density $\rho_{\rm nuc}$ and mobility $B$ on power law exponent: when $\dot{\sigma} = E^* * 10^2$/s, changing $\rho_{\rm nuc}$ from $60\mu$m$^2$ (purple curve) to $15\mu$m$^2$ (blue curve) leads to the exponent changing from 2.5 to 2.1. Increasing $B$ from $10^{-4}$ Pa.s to $10^{-3}$ Pa.s results in the change of exponent from 2.5 to 2.2.

ing rates: Fig. 3(a) shows avalanche statistics for different stress rate which varies from $\dot{\sigma} = E^* * 10$/s to $\dot{\sigma} = E^* * 10^4$/s. Power law events distribution appear for all stress rates, yet with different exponent which changes from 3.5 for $\dot{\sigma} = E^* * 10$/s to -1.5 for $\dot{\sigma} = E^* * 10^4$/s (See also SI). The dependence of the exponent on the stress rate indicates that there is an intrinsic connec-

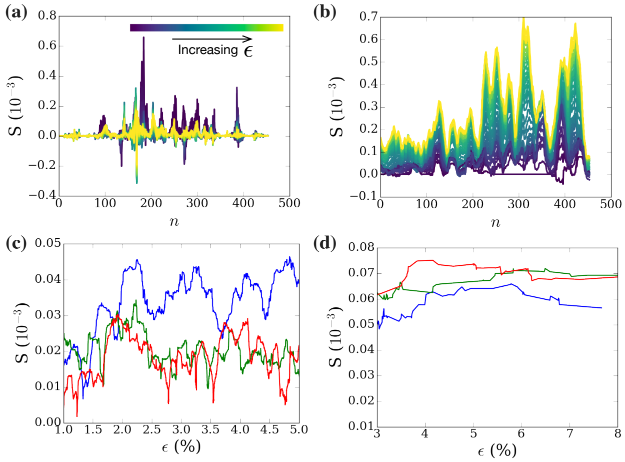


FIG. 4: **Spatial and temporal event distribution in SC.** Event distribution on all slip planes during the loading up to 10% strain for $\dot{\sigma} = E^* {*} 10^2$ (**(a)**) and for $\dot{\sigma} = E^* {*} 10^4$ (**(b)**): $n$ is the total number of slip planes in the model. The color changes from dark purple to yellow with increasing loading strain. **(c)**: Average avalanche size for $\dot{\sigma} = E^* * 10^2$ in a single sample. **(d)**: Average avalanche size for $\dot{\sigma} = E^* * 10^4$ in a single sample.

tion between event statistics and dislocation drag. In order to verify the connection, for the same stress rate $\dot{\sigma} = E^* {*} 10^2$/s , in Fig. 3(b) red curve, we increase the dislocation mobility $B$ by which the drag effect is enhanced, it is seen that the exponent changes from 2.5 to 2.2. Dislocation drag effect will also magnify when dislocation nucleation effect is weakened due possibly to dislocation cross-slip and other mechanisms (since the main source of plasticity will be the moving of dislocations instead of nucleations of new dislocations). This can be seen in Fig. 3(b) blue curve, when lower dislocation source density is used, the exponent changes from 2.5 to 2.1.

Power law avalanche behavior in the elastic depinning of disordered systems has been well established [29, 34–36, 87]. However, crystal plasticity is known to be unstable to strain localization which adds an inhomogeneity effect to power-law behaviors [89]. In Fig. 4(a) and (b), we plot events spatial distribution along all slip planes for the whole loading process (from small $\epsilon$ to large $\epsilon$ which is represented by the color map from purple to yellow). Fig. 4(a) shows the event spatial distribution for a smaller loading rate ($\dot{\sigma} = E^* * 10^2$). It can be seen that events are localized around certain slip planes, moreover, events do not always happen at the same slip planes. By contrast, the event distribution shown in Fig. 4(b) for higher loading rate ($\dot{\sigma} = E^* * 10^4$) is more uniform among slip planes, resembling a moving "interface". This inhomogeneity effect can be also seen by the behavior of the event size with increasing strain (S vs. time): Oscillatory-like behavior emerges for small stress rate shown in Fig. 4(c) while no periodicity is observed for higher stress rate. These results are strikingly similar to the avalanche behavior reported in Ref. [41].

The onset of inhomogeneous response at small rates in the absence of overall weakening in this model is the outcome of an interplay between two timescales (as in other elasticity models [37]) and a characteristic feature of small volumes, since in that case, it is true that boundaries (free) may absorb propagating dislocations. Due to this property, it is natural to expect an integration of avalanche behaviors, dependent on the resetting behavior that emerges from absorption and re-nucleation of dislocations at various slip planes. The overall effect can be thought of as originating within a relaxation process (nucleation) that contributes to slip, in addition to mobile dislocation motion. This is the type of coarse-grained dislocation modeling that was pursued in Ref. [41] and its analysis leads to critical power law exponents that are higher than mean-field ones ($\sim 3/2$). Local heterogeneity biases the integration of the size probability distribution of the conventional depinning models. In this paper, through dislocation dynamics simulations, we connect plasticity local heterogeneity to strain rate effect: the lower loading rate results in the higher heterogeneity which leads to a higher power law exponent. If $P(S,k) \sim S^{-\tau_0} e^{-kS}$, with $k$ a cutoff parameter, then an effective *integrated* distribution emerges:

$$P_{int}(S) = \int_0^\infty g(k')P(S,k')dk' \tag{1}$$

where $g(k')$ is the weight factor that characterizes the contribution of various sub-critical, quasi-localized spatial contributions to slip events and depends on the applied loading rate. This weight factor $g(k')$ contains a natural $k' \to 0$ limit, due to the quasi-periodic resetting, which in many cases takes the form of a power-law [41], thus identifying a novel exponent $g(k') \sim k'^{\alpha}$. Thus, for the critical aspect of $P_{int}(S) \sim S^{-\tau_0-\alpha-1}$, with the ultimate avalanche size exponent being,

$$\tau = \tau_0 + \alpha + 1 \tag{2}$$

For the current model, by the analysis of Figs. 4(a, b), we can estimate $\alpha$: If we assume that each 3 nearby slip planes are locally independent from the rest of the system, then the max event size in that area can provide an estimate of the cutoff scale ($k_0 \sim 1/S_0$). Then, the distribution of $k_0$'s provides the exponent. We find that $\alpha \simeq 1$ by plotting the histogram of events that considering $\tau_0 \simeq 1.5$. However, the statistics has not been adequate to justify a precise exponents' identification.

Our model is limited to small deformations, and does not include boundary roughness stress effects, or thermal effects on obstacles/sources [93, 94]. However, it is interesting to compare the statistical behavior of this model to mean-field plasticity avalanche behaviors, which may emerge in disordered materials or granular systems [28, 92]. We find (*cf.* Table *II*) that free nanoscale boundaries and competition between dislocation nucleation and drag conspire to give quasi-periodic avalanche bursts. The behavior is akin to a mean-field integrated behavior [32], as the strain-rate *decreases*, and it was originally labeled as *avalanche oscillator* [41]. In this model, at low strain-rates, critical exponents $\tau$ and $\alpha$ are higher than ~~typical~~ mean-field, but the spectral density one $x$ [90] remains at its mean-field limit at low rates (see SI) while x' ($\langle S\rangle \sim T^{x'}$) implies integrated mean-field behavior [90] (*cf.* Table II). This novel behavior might explain large exponents in crystal plasticity of small grains in polycrystals [91] or crystalline pillar experiments [72].

TABLE II: **Universality and Exponents**. Basic mean-field avalanche exponents characterize power-law behaviors in avalanche sizes $P(S) \sim S^{-\tau}$, durations $P(T) \sim T^{-\alpha}$, spectral response $S(\omega) \sim \omega^{-x}$ and average size-duration relationship $\langle S\rangle \sim T^{x'}$.

| Exponent | Mean-Field Theory | Avalanche Oscillator |
|---|---|---|
| $\tau$ | 3/2 | Rate-Dependent> 3/2 |
| $\alpha$ | 2 | Rate-Dependent> 2 |
| $x$ | 2 | 2 |
| $x'$ | 2 | 1 |

We would like to thank I. Groma, P. Ispanovity, R. Maass, L. Ponson for encouraging and insightful comments. This work is supported through awards DOC - No. 1007294R (SP) and DOE-BES DE-SC0014109.

[1] J. R. Greer and J. T. M. De Hosson, Progress in Materials Science **56**, 654 (2011).
[2] M. D. Uchic, P. A. Shade, and D. M. Dimiduk, Annual Review of Materials Research **39**, 361 (2009).
[3] J. R. Greer, W. C. Oliver, and W. D. Nix, Acta Materialia **53**, 1821 (2005).
[4] J. R. Greer and W. D. Nix, Physical Review B **73**, 245410 (2006).
[5] I. Ryu, W. Cai, W. D. Nix, and H. Gao, Acta Materialia **95**, 176 (2015).
[6] J. Krebs, S. Rao, S. Verheyden, C. Miko, R. Goodall, W. Curtin, and A. Mortensen, Nature materials **16** (2017).
[7] M. F. Doerner and W. D. Nix, Journal of Materials research **1**, 601 (1986).
[8] W. D. Nix and H. Gao, Journal of the Mechanics and Physics of Solids **46**, 411 (1998).
[9] J. J. Vlassak and W. Nix, Philosophical Magazine A **67**, 1045 (1993).
[10] M. R. Begley and J. W. Hutchinson, Journal of the Mechanics and Physics of Solids **46**, 2049 (1998).
[11] Y. Wei and J. W. Hutchinson, Journal of the Mechanics and Physics of Solids **51**, 2037 (2003).
[12] J. W. Hutchinson, International Journal of Solids and Structures **37**, 225 (2000).
[13] M. D. Uchic, D. M. Dimiduk, J. N. Florando, and W. D. Nix, Science **305**, 986 (2004).
[14] M. D. Uchic, D. M. Dimiduk, J. N. Florando, and W. D. Nix, MRS Online Proceedings Library Archive **753** (2002).
[15] N. Fleck and J. Hutchinson, Journal of the Mechanics and Physics of Solids **49**, 2245 (2001).
[16] E. C. Aifantis, Journal of Engineering Materials and technology **106**, 326 (1984).
[17] E. C. Aifantis, *Strain gradient interpretation of size effects* (Springer, 1999), pp. 299–314.
[18] P. M. Anderson, J. P. Hirth, and J. Lothe, *Theory of dislocations* (Cambridge University Press, 2017), ISBN 0521864364.
[19] B. Devincre, T. Hoc, and L. Kubin, Science **320**, 1745 (2008).
[20] F. F. Csikor, C. Motz, D. Weygand, M. Zaiser, and S. Zapperi, Science **318**, 251 (2007).
[21] D. M. Dimiduk, C. Woodward, R. LeSar, and M. D. Uchic, Science **312**, 1188 (2006).
[22] M.-C. Miguel, A. Vespignani, S. Zapperi, J. Weiss, and J.-R. Grasso, Nature **410**, 667 (2001).
[23] R. Maaß, P. M. Derlet, and J. R. Greer, Scripta Materialia **69**, 586 (2013).
[24] M. Koslowski, R. LeSar, and R. Thomson, Physical review letters **93**, 125502 (2004).
[25] P. Sammonds, Nature materials **4**, 425 (2005).
[26] C. R. Weinberger and W. Cai, Proceedings of the National Academy of Sciences (2008).
[27] J. A. El-Awady, S. I. Rao, C. Woodward, D. M. Dimiduk, and M. D. Uchic, International Journal of Plasticity **27**, 372 (2011).
[28] J. T. Uhl, S. Pathak, D. Schorlemmer, X. Liu, R. Swindeman, B. A. Brinkman, M. LeBlanc, G. Tsekenis, N. Friedman, R. Behringer, et al., Scientific reports **5**, 16493 (2015).
[29] D. S. Fisher, K. Dahmen, S. Ramanathan, and Y. Ben-Zion, Physical review letters **78**, 4885 (1997).
[30] Y. Ben-Zion, Reviews of Geophysics **46** (2008).
[31] A. L. Demirel and S. Granick, Physical review letters **77**, 4330 (1996).
[32] S. Papanikolaou, Y. Cui, and N. Ghoniem, Modelling and Simulation in Materials Science and Engineering **26**, 013001 (2017).
[33] P. D. Ispánovity, L. Laurson, M. Zaiser, I. Groma, S. Zapperi, and M. J. Alava, Physical review letters **112**, 235501 (2014).
[34] M. Zaiser and P. Moretti, Journal of Statistical Mechanics: Theory and Experiment **2005**, P08004 (2005).
[35] M. Zaiser, Advances in physics **55**, 185 (2006).
[36] K. A. Dahmen, Y. Ben-Zion, and J. T. Uhl, Physical review letters **102**, 175501 (2009).
[37] E. Jagla and A. Kolton, Journal of Geophysical Research: Solid Earth **115** (2010).
[38] P. Moretti, M.-C. Miguel, M. Zaiser, and S. Zapperi, Physical Review B **69**, 214103 (2004).
[39] Z. Shan, R. K. Mishra, S. S. Asif, O. L. Warren, and A. M. Minor, Nature materials **7**, 115 (2008).
[40] V. Bulatov and W. Cai, *Computer simulations of dislocations*, vol. 3 (Oxford University Press on Demand, 2006), ISBN 0198526148.
[41] S. Papanikolaou, D. M. Dimiduk, W. Choi, J. P. Sethna, M. D. Uchic, C. F. Woodward, and S. Zapperi, Nature **490**, 517 (2012).

[42] E. Jagla, Physical Review E **81**, 046117 (2010).
[43] E. Jagla, Physical Review E **76**, 046119 (2007).
[44] Y. Cui, G. Po, and N. Ghoniem, Physical review letters **117**, 155502 (2016).
[45] J. Weiss, F. Lahaie, and J. R. Grasso, Journal of Geophysical Research: Solid Earth **105**, 433 (2000).
[46] C. Fressengeas, A. Beaudoin, D. Entemeyer, T. Lebedkina, M. Lebyodkin, and V. Taupin, Physical Review B **79**, 014108 (2009).
[47] J. Weiss, T. Richeton, F. Louchet, F. Chmelik, P. Dobron, D. Entemeyer, M. Lebyodkin, T. Lebedkina, C. Fressengeas, and R. J. McDonald, Physical review B **76**, 224110 (2007).
[48] N. Friedman, A. T. Jennings, G. Tsekenis, J.-Y. Kim, M. Tao, J. T. Uhl, J. R. Greer, and K. A. Dahmen, Physical review letters **109**, 095507 (2012).
[49] P. D. Ispánovity, I. Groma, G. Györgyi, F. F. Csikor, and D. Weygand, Physical review letters **105**, 085503 (2010).
[50] M.-C. Miguel, A. Vespignani, M. Zaiser, and S. Zapperi, Physical review letters **89**, 165501 (2002).
[51] M.-C. Miguel, A. Vespignani, S. Zapperi, J. Weiss, and J.-R. Grasso, Materials Science and Engineering: A **309**, 324 (2001).
[52] P. Moretti, M.-C. Miguel, M. Zaiser, and S. Zapperi, Physical Review B **69**, 214103 (2004).
[53] S. Zapperi and M. Zaiser, Materials Science and Engineering: A **309**, 348 (2001).
[54] L. Laurson and M. J. Alava, Physical Review E **74**, 066106 (2006).
[55] L. Laurson, M.-C. Miguel, and M. J. Alava, Physical review letters **105**, 015501 (2010).
[56] M. Ovaska, L. Laurson, and M. J. Alava, Scientific reports **5**, 10580 (2015).
[57] I. Groma, G. Györgyi, and P. Ispanovity, Physical review letters **108**, 269601 (2012).
[58] G. Tsekenis, N. Goldenfeld, and K. A. Dahmen, Physical review letters **106**, 105501 (2011).
[59] O. U. Salman and L. Truskinovsky, Physical review letters **106**, 175503 (2011).
[60] O. U. Salman and L. Truskinovsky, International Journal of Engineering Science **59**, 219 (2012).
[61] S. Kale and M. Ostoja-Starzewski, Physical review letters **112**, 045503 (2014).
[62] P. D. Ispánovity, Á. Hegyi, I. Groma, G. Györgyi, K. Ratter, and D. Weygand, Acta Materialia **61**, 6234 (2013).
[63] T. A. Parthasarathy, S. I. Rao, D. M. Dimiduk, M. D. Uchic, and D. R. Trinkle, Scripta Materialia **56**, 313 (2007).
[64] S. I. Rao, D. Dimiduk, T. A. Parthasarathy, M. Uchic, M. Tang, and C. Woodward, Acta Materialia **56**, 3245 (2008).
[65] M. Stricker and D. Weygand, Acta Materialia **99**, 130 (2015).
[66] T. Crosby, G. Po, C. Erel, and N. Ghoniem, Acta Materialia **89**, 123 (2015).
[67] H. Swan, W. Choi, S. Papanikolaou, M. Bierbaum, Y. S. Chen, and J. P. Sethna, Materials Theory **2**, 5 (2018), URL `https://doi.org/10.1186/s41313-018-0012-x`.
[68] G. Tsekenis, J. T. Uhl, N. Goldenfeld, and K. A. Dahmen, EPL (Europhysics Letters) **101**, 36003 (2013).
[69] J. Weiss, W. B. Rhouma, T. Richeton, S. Dechanel, F. Louchet, and L. Truskinovsky, Physical review letters **114**, 105504 (2015).
[70] P. Zhang, O. U. Salman, J.-Y. Zhang, G. Liu, J. Weiss, L. Truskinovsky, and J. Sun, Acta Materialia **128**, 351 (2017).
[71] R. Maaß, M. Wraith, J. Uhl, J. Greer, and K. Dahmen, Physical Review E **91**, 042403 (2015).
[72] G. Sparks and R. Maass, Acta Materialia **152**, 86 (2018).
[73] R. Armstrong and S. Walley, International Materials Reviews **53**, 105 (2008).
[74] W. Murphy, A. Higginbotham, G. Kimminau, B. Barbrel, E. Bringa, J. Hawreliak, R. Kodama, M. Koenig, W. McBarron, M. Meyers, et al., Journal of Physics: Condensed Matter **22**, 065404 (2010).
[75] W. Tong, R. J. Clifton, and S. Huang, Journal of the Mechanics and Physics of Solids **40**, 1251 (1992).
[76] R. J. Clifton, International Journal of Solids and Structures **37**, 105 (2000).
[77] P. K. Agnihotri and E. Van der Giessen, Mechanics of Materials **90**, 37 (2015).
[78] J. Hu, Z. Liu, E. Van der Giessen, and Z. Zhuang, Extreme Mechanics Letters **17**, 33 (2017).
[79] J. P. Hirth and J. Lothe (1982).
[80] S. Papanikolaou, H. Song, and E. Van der Giessen, Journal of the Mechanics and Physics of Solids **102**, 17 (2017).
[81] E. Van der Giessen and A. Needleman, Modelling and Simulation in Materials Science and Engineering **3**, 689 (1995).
[82] P. S. Sahni, D. J. Srolovitz, G. S. Grest, M. P. Anderson, and S. Safran, Physical Review B **28**, 2705 (1983).
[83] Y. Xiang and J. Vlassak, Acta Materialia **54**, 5449 (2006).
[84] L. Nicola, Y. Xiang, J. Vlassak, E. Van der Giessen, and A. Needleman, Journal of the Mechanics and Physics of Solids **54**, 2089 (2006).
[85] P. Follansbee and U. Kocks, Acta Metallurgica **36**, 81 (1988).
[86] R. Clifton, Applied mechanics reviews **43**, S9 (1990).
[87] K. A. Dahmen, Y. Ben-Zion, and J. T. Uhl, Nature Physics **7**, 554 (2011).
[88] D. S. Fisher, Physics reports **301**, 113 (1998).
[89] R. Asaro and V. Lubarda, *Mechanics of solids and materials* (Cambridge University Press, 2006), ISBN 1139448994.
[90] S. Papanikolaou, F. Bohn, R-L. Sommer, G. Durin, S. Zapperi, J. P. Sethna, Nature Physics, 7, 316 EP, 2011.
[91] T. A. Lebedkina, D. A. Zhemchuzhnikova and M. A. Lebyodkin, Phys. Rev. E, **97**, 013001 (2018).
[92] S. Papanikolaou, Physical Review E, 93(3), p.032610 (2016).
[93] H. Song, H. Yavas, E. Van der Giessen, S. Papanikolaou, Journal of the Mechanics and Physics of Solids, **123**, p.332 (2019)
[94] S. Papanikolaou, M. Tzimas, A. Reid, S. Langer (Phys. Rev. E under review)
[95] this process mimics the physical process of Frank Read source multiplication
[96] thus, the plastic strain generate by a nucleated dipole (which will be put at 35nm apart along a 60 degree slip plane) is $b * sin60^{\circ}/h * 35nm * cos60^{\circ}/w \simeq 10^{-6}$